

Article

Temporal and Spatial Distribution Characteristics of Drought and Its Influence on Vegetation Change in Xilin Gol, China

Zexun Chen ^{1,2}, Wenjun Wang ^{1,2}, Yingjie Wu ^{1,2,*}, Hang Yin ^{1,2}, Wei Li ^{1,2} and Shuixia Zhao ¹

¹ Yinshanbeilu National Field Research Station of Desert Steppe Eco-Hydrological System, China Institute of Water Resources and Hydropower Research, Beijing 100038, China

² Institute of Water Resources for Pastoral Area Ministry of Water Resources, Hohhot 010020, China

* Correspondence: wuyj@iwhr.com

Abstract: Drought hinders economic and social growth in many areas of China, especially in livestock-dominated Xilin Gol League in Inner Mongolia. Most studies exclusively utilize rainfall to measure drought. To clarify the spatial and temporal distribution characteristics and evolution rules of meteorological drought, monthly observation data from nine meteorological stations in Xilin Gol were used to calculate the (effective drought index, *EDI*). We studied the spatiotemporal pattern of drought and its influence on vegetation in Xilin Gol using the Mann–Kendall test, (empirical orthogonal function, EOF) decomposition, and quantitative representation. (1) The annual average *EDI* declined by 0.029/10a, and Xilin Gol experienced an average of 0.5 drought occurrences every year. (2) A normal incidence in Xilin Gol is 67.17–72.65%, and that of severe drought is 0.02–0.99%. (3) Xilin Gol's drought intensity is mostly concentrated in the central, northeast, and southwest regions, especially southwest and central. (4) The first two principal feature vectors in Xilin Gol contributed 52.75% and 14.38% to the variance. (5) The average (normalized differential vegetation index, NDVI) of desert, typical, and meadow steppe increased, especially in typical steppe (0.034/10a). (6) In Xilin Gol, the NDVI–*EDI* correlation coefficient ranges from –0.642 to 0.888, with an average of 0.392. Only 1.7% of the areas are adversely linked.

Keywords: effective drought index; drought; vegetation index; grass; drought event



Citation: Chen, Z.; Wang, W.; Wu, Y.; Yin, H.; Li, W.; Zhao, S. Temporal and Spatial Distribution Characteristics of Drought and Its Influence on Vegetation Change in Xilin Gol, China. *Atmosphere* **2022**, *13*, 1743. <https://doi.org/10.3390/atmos13111743>

Academic Editors: Shuyao Wu and Wentao Zhang

Received: 18 September 2022

Accepted: 17 October 2022

Published: 22 October 2022

Publisher's Note: MDPI stays neutral with regard to jurisdictional claims in published maps and institutional affiliations.



Copyright: © 2022 by the authors. Licensee MDPI, Basel, Switzerland. This article is an open access article distributed under the terms and conditions of the Creative Commons Attribution (CC BY) license (<https://creativecommons.org/licenses/by/4.0/>).

1. Introduction

Grassland is one of the most widely distributed vegetation types in the world, covering one-fifth of the Earth's land surface. Due to climate change, population growth, and socioeconomic development, more than half of the grassland in China has been degraded to varying degrees [1,2]. Grassland degradation has reduced carbon sequestration and led to serious environmental and social problems, such as reduced vegetation productivity and soil quality, as well as dust storms [3,4]. Drought is a natural disaster that can occur in any area [5,6]. Agriculture, animal husbandry, water resources, and society are impacted. Drought is increasing due to global warming. It impacts Inner Mongolian agriculture and livestock [7]. Drought evaluation and monitoring are necessary to limit damage and safeguard people's safety. Even though drought is complex, it can be characterized by drought indices, such as the standardized precipitation index (SPI) [8–11], standardized precipitation evapotranspiration index (SPEI) [12–15], reconnaissance drought index (RDI) [16], Palmer drought severity index (PDSI) [17–19], and effective drought index (*EDI*) [20]. The drought index can be quantitatively described by basic attributes such as intensity, event, and frequency [21]. The most popular approach is SPI. SPI is estimated using cumulative rainfall probability, which has limits. SPEI considers rainfall and potential evapotranspiration to estimate drought severity [22]. Using different potential evapotranspiration calculation methods leads to varied SPEI results [23]. *EDI* was created to circumvent these restrictions, representing a milestone in drought research. *EDI*'s use of rainfall data makes

it more representative of drought conditions than other indices and able to reflect the genuine nature of drought in the research area. Some studies have shown the suitability of *EDI*. In particular, ref. [24] demonstrated the advantages of *EDI* over *SPI* when monitoring long-term and short-term droughts in Bangladesh.

One of many drought indices, *SPEI* is widely used to analyze the response of vegetation to drought. At present, scholars across the world have carried out many studies on the response of vegetation growth to drought. For example, Wang et al. [25] explored the correlation between *NDVI* and drought index at the whole watershed scale in China and found that the two showed strong positive correlation in arid and semi-arid areas. Similar positive correlations were also found in other semi-arid areas around the world, and the increase in *NDVI*_{max} was accompanied by a significant increase in drought index in these areas [26]. However, the response of different vegetation types to drought was also different, and the larger drought index was not conducive to the growth of vegetation [27]. However, *EDI* has not been used to analyze the vegetation response to drought when studying the vegetation response to drought.

Grassland is a major form of vegetation in China, and it plays a vital role in maintaining regional ecological balance and climatic management. Grassland is more vulnerable to drought than other vegetation species, according to studies, and the resistance and resilience stability of different grassland types to water scarcity and climate dryness are extremely variable. Due to their shape and phenological patterns, grassland ecosystems, for example, are exposed to drought and semi-arid settings for a long period and often demonstrate significant drought resistance and stress tolerance after drought circumstances end [28]. As a result, it is critical to investigate the drought response mechanisms of various grassland types in order to conserve and care for grassland resources. Many researchers have researched the drought characteristics of Xilin Gol using the *SPI* and *SPEI* [29,30]; however, the *EDI* has not been employed to define drought event characteristics. As a result, this study used monthly rainfall data from the study area's meteorological site from 1969 to 2018, and *EDI* was chosen as the evaluation index, along with drought and the normalized difference vegetation index (*NDVI*), as the regional scale representation of green vegetation and dynamic stability index, from the drought event, drought frequency, and intensity of drought, according to the quantitative description of drought characteristics. Second, in Xilin Gol, the empirical orthogonal function (*EOF*) was employed to investigate the geographical and temporal distribution characteristics of drought. Finally, in order to give a reference for ecological environment conservation and vegetation restoration in the research region, the response connection of vegetation change to drought status during the last 19 years was analyzed.

2. Study Area and Methods

2.1. Study Area

Xilin Gol League, which can be found in the middle of the Inner Mongolia Autonomous Region and has a geographical position ranging from 111°08' to 120°07' east and 41°35' to 46°40' north, is not only one of China's four natural pastures but also an example of a typical temperate continental grassland found in the country. The topography is mostly composed of high plains, and it varies in elevation from south to north. There are also alternating patterns of different types of landforms. The area has an arid and semi-arid continental monsoon climate, with annual precipitation ranging from 300 to 380 mm, increasing from southwest to northeast, with rainfall primarily focused from June to August. The altitude ranges from 700 to 2000 m (Figure 1b). Figure 1 illustrates both the overall distribution of meteorological stations, as well as their individual locations.

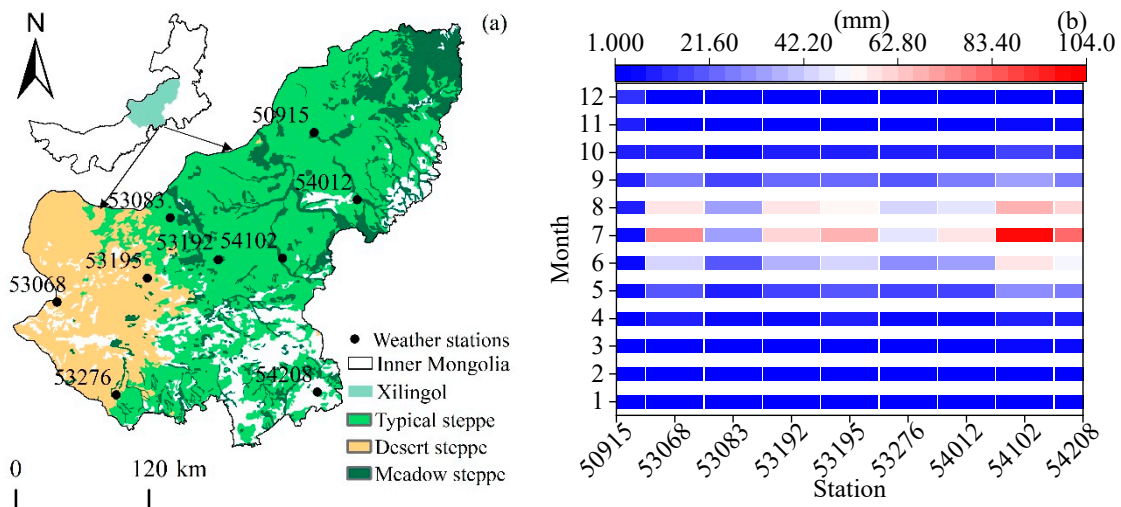


Figure 1. (a) Map of the study area of the Xilin Gol Region of China showing distribution of study area and meteorological stations. (b) Monthly rainfall changes at different stations from 1969 to 2018. (50,915: Dong Ujimqin Banner, 53,068: Erenhot, 53,083: Naran-Bulag, 53,192: Abag Banner, 53,195: Sonid Left Banner, 53,276: Zhurihe, 54,012: Xi Ujimqin Banner, 54,102: Xilin Hot, and 54,208: Duolun).

2.2. Data Sources

The meteorological data were obtained from the China Meteorological Data Sharing Network <http://data.cma.cn/> (accessed on 1 June 2022), including monthly rainfall data of nine meteorological stations in Xilin Gol region from 1969 to 2018 (Figure 1a), mainly to calculate the drought index.

2.3. Effective Drought Index

EDI uses the precipitation of the current and antecedent months’ precipitation over time and assigns different weights to monthly precipitation to assess the cumulative level of precipitation needed to supplement the accumulated losses since the onset of drought [31]. The calculation procedure is as follows.

First, water stored due to precipitation accumulates over a year, while losses due to evaporation are also taken into account:

$$EP_i = \sum_{n=1}^i \left[\left(\sum_m^n P_m \right) / n \right] \tag{1}$$

where P_m is the precipitation before month m , and 12 is taken as the preset value of i , which is the most used water cycle. Therefore, is the cumulative value of available precipitation on the time scale of December.

Secondly, the difference between the monthly cumulative effective precipitation and the average effective rainfall is calculated using the following formula:

$$DEP = EP - MEP \tag{2}$$

where (mean effective precipitation, MEP) is the average effective precipitation of each month, (effective precipitation, EP) is the monthly cumulative effective precipitation, and (deviation of EP , DEP) is the difference between the monthly cumulative effective precipitation and the average effective rainfall in the same period of 50 years.

$$EDI = DEP / ST(DEP) \tag{3}$$

Here, EDI stands for the effective drought index, and (standard, ST) (DEP) is the standard deviation of the difference between the monthly cumulative effective precipitation

and the average effective rainfall over the same period of 50 years. When the *DEP* number is negative, it indicates that the climate is drier than normal. Equations (1) and (3) are recalculated, and the drought grade is categorized according to the *EDI* classification technique suggested by Byun et al. (2010), as can be seen in Table 1, if the number of consecutive months with a negative *DEP* is more than 12 months. In addition, drought episodes, drought frequency, and drought severity were computed in order to provide a quantitative description of the drought that has been affecting Xilin Gol.

Table 1. Drought classes of meteorological drought indices.

Drought Grade	Drought Definition	EDI Value
1	Normal	$-1 < EDI \leq 1$
2	Mild drought	$-1.5 < EDI \leq -1$
3	Moderate drought	$-2 < EDI \leq -1.5$
4	Severe drought	$EDI \leq -2$

2.4. Quantitative Characterization of Drought

The quantitative representation of drought is expressed by its attributes, which mainly include drought frequency and drought intensity.

(1) Drought frequency

Drought frequency is the proportion of the number of months with drought in the total number of months in the study period, and the larger the value, the more frequently the drought occurs.

$$P = (m/M) \times 100\% \tag{4}$$

Here, *m* is the number of months in which drought occurs, and *M* is the total number of months.

(2) Drought intensity

Drought intensity was used to evaluate the severity of drought in the study area. In the process of drought, the *EDI* value of drought to light drought is recorded as the cumulative value of 1.5; the larger the value, the stronger the drought.

$$Q = \sum EDI_{EDI \leq -1.5} \tag{5}$$

Here, $EDI_{EDI \leq -1.5}$ is an *EDI* value less than -1.5 .

2.5. Mann–Kendall Test

For the time series $X = \{x_1, x_2, \dots, x_n\}$ with sample size *n*, a statistical variable S_k is constructed [32]. S_k is the cumulative number of values at time *i* of the sample greater than that at time *j*:

$$S_k = \sum_{i=1}^k r_i, \quad k = 2, 3, \dots, n \tag{6}$$

$$r_i = \begin{cases} +1, & \text{when } x_i > x_j \\ 0, & \text{when } x_i \leq x_j \end{cases} \quad (j = 1, 2, \dots, i) \tag{7}$$

Assuming that the time series *X* is random and independent and approximately follows a normal distribution, the statistic UF_k is defined as:

$$UF_k = \frac{S_k - E(S_k)}{\sqrt{Var(S_k)}} \quad k = 1, 2, \dots, n \tag{8}$$

$$Var(S_k) = \frac{k(k-1)(2k+5)}{72} \tag{9}$$

$$E(S_k) = \frac{k(k-1)}{4} \tag{10}$$

where $E(S_k)$ and $Var(S_k)$ are the mean and variance of the cumulative number, respectively, and the mean and variance of the cumulative number S_k . UF_k is a standard normal distribution; given a significance level α , if $|UF_k| > U\alpha/2$, it indicates a clear trend in the series.

2.6. Empirical Orthogonal Function Decomposition

From complicated drought variable fields, several spatial and temporal modes may be extracted using empirical orthogonal function decomposition [33,34].

- (1) Select the data to be analyzed and preprocess the data.

Generally, the original data matrix X is processed by an anomaly to obtain the data matrix $X_{m \times n}$. The product of the matrix $X_{m \times n}$ and its transpose matrix is calculated to obtain:

$$C_{m \times m} = \frac{1}{n} (X_{m \times n} X_{m \times n}^T) \tag{11}$$

where $C_{m \times m}$ is the covariance matrix, $X_{m \times n}$ is the data matrix, m is the weather station, and n is the year.

- (2) Calculate the eigenvalues and eigenvectors of the matrix $C_{m \times m}$.

The following must be met:

$$C_{m \times m} \times V_{m \times m} = V_{m \times m} \times E_{m \times m} \tag{12}$$

where $V_{m \times m}$ is the eigenvector of matrix $C_{m \times m}$, and $E_{m \times m}$ is the diagonal matrix of $m \times m$, namely:

$$E_{m \times m} = \begin{pmatrix} \lambda_1 & 0 & \dots & 0 \\ 0 & \lambda_2 & \dots & 0 \\ \vdots & \vdots & \vdots & \vdots \\ 0 & 0 & \dots & \lambda_m \end{pmatrix} \tag{13}$$

where $\lambda_1, \lambda_2 \dots \lambda_m$ is the eigenvalue of matrix $C_{m \times m}$. The eigenvalues are arranged from largest to smallest, and a column of eigenvectors corresponding to each nonzero eigenvalue is regarded as a spatially distributed mode corresponding to EOF.

- (3) Calculate the time coefficient matrix.

The time coefficient matrix can be calculated from the eigenvectors in the matrix $C_{m \times m}$. After $V_{m \times m}$, the time coefficient matrix can be obtained as follows:

$$T_{m \times n} = V_{m \times m}^T \times X_{m \times n} \tag{14}$$

where $T_{m \times n}$ is the time coefficient matrix.

In this study, the Mann–Kendall test and empirical orthogonal function decomposition were performed with MATLAB (2020b, MathWorks, Torrance, CA, USA), and the spatial distribution map was drawn using the inverse distance weight method in ArcGIS (10.6, ESRI, RedLands, CA, USA).

3. Results

3.1. Variation Characteristics of Meteorological Drought in Xilin Gol

3.1.1. Interannual Variation and Mutation Detection of Drought

The annual average *EDI* value of Xilin Gol is the average value of nine meteorological stations, and all stations are evenly distributed in each area of Xilin Gol, providing good representation. It can be seen from Figure 2a that, from 1969 to 2018, the annual average *EDI* in Xilin Gol decreased at a rate of 0.029/(10 a), and the drought trend was significantly enhanced. During 1980–2000, the *EDI* value was generally greater than 0, indicating a

stable period, while, during 1970–1980, the change was very drastic, indicating that the alteration between dry and wet was quite obvious during this period. On the whole, the *EDI* changed between -1.5 and 1.5 . From 1969 to 2018, there were 0.5 drought events in Xilin Gol every year on average. Among them, the year 2000 was the most prominent, with moderate drought, severe drought, and the total number of drought events being 2.3 times in total.

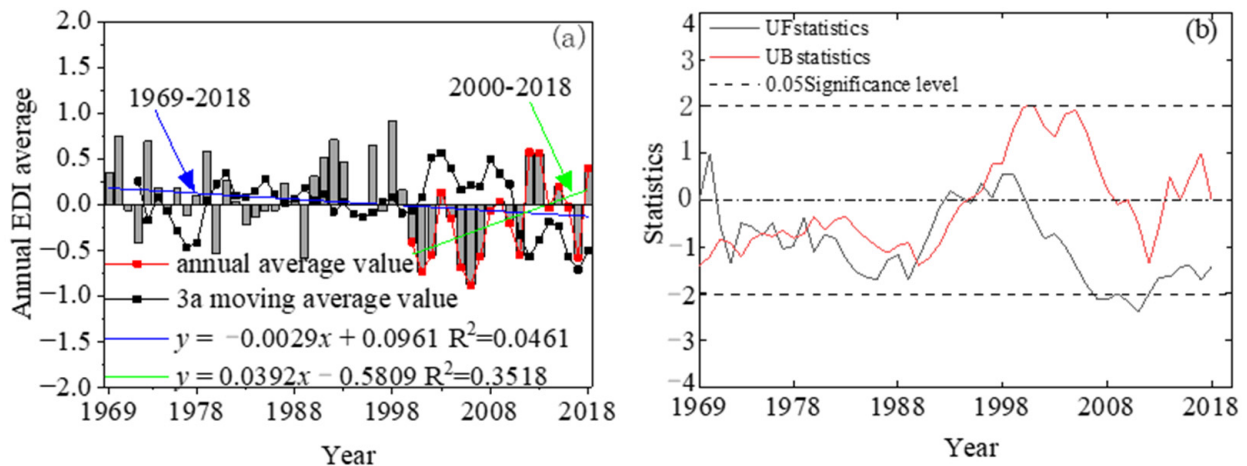


Figure 2. (a) Interannual variation characteristics of 1969–2018 *EDI*. (b) *EDI* interannual Mann–Kendall Test.

Figure 2b shows the M–K test results of the Xilin Gol effective drought index. As can be seen from the figure, there were six intersections between the positive sequence curve UF and the negative sequence curve UB during 1969–2000, namely 1972, 1974, 1978, 1980, 1990, and 1995. However, none of these intersections exceeded the 0.05 significance line. Only 1995 was found to be a significant mutation year according to the sliding *t*-test. The *EDI* value in 1995 was 0.78. The period after 2000 was mainly dry.

3.1.2. Spatial Distribution Characteristics of Drought

The geographical distribution of the occurrence frequency of the various drought classes is depicted in Figure 3, which can be seen here. In Xilin Gol, the frequency of normal occurrence spans from 67.17% to 72.65%, while the frequency of severe drought ranges from 0.02% to 0.99%, as shown in the figure. There is a significant disparity in the frequency of the various droughts. It is more likely for there to be a drought in the west, northwest, and southeast regions of Xilin Gol, especially a mild drought, than in the center and northeast regions. In general, the frequency of drought in the northwest of Xilin Gol is higher than that in the west and southeast of Xilin Gol, which has clear zone characteristics. This is because the northwest of Xilin Gol is more exposed to the elements. The regions that have a high incidence of brief droughts are primarily located in close proximity to Nalemlige and Zhurihe. The highest concentration of locations is found near Duolun, with a high incidence of severe drought. The regions of Duolun and Erenhot mostly have a high incidence of severe droughts. Since the temperature and amount of precipitation in Xilin Gol are not consistently distributed in space from one location to the next, different degrees of drought can occur with varying regularity.

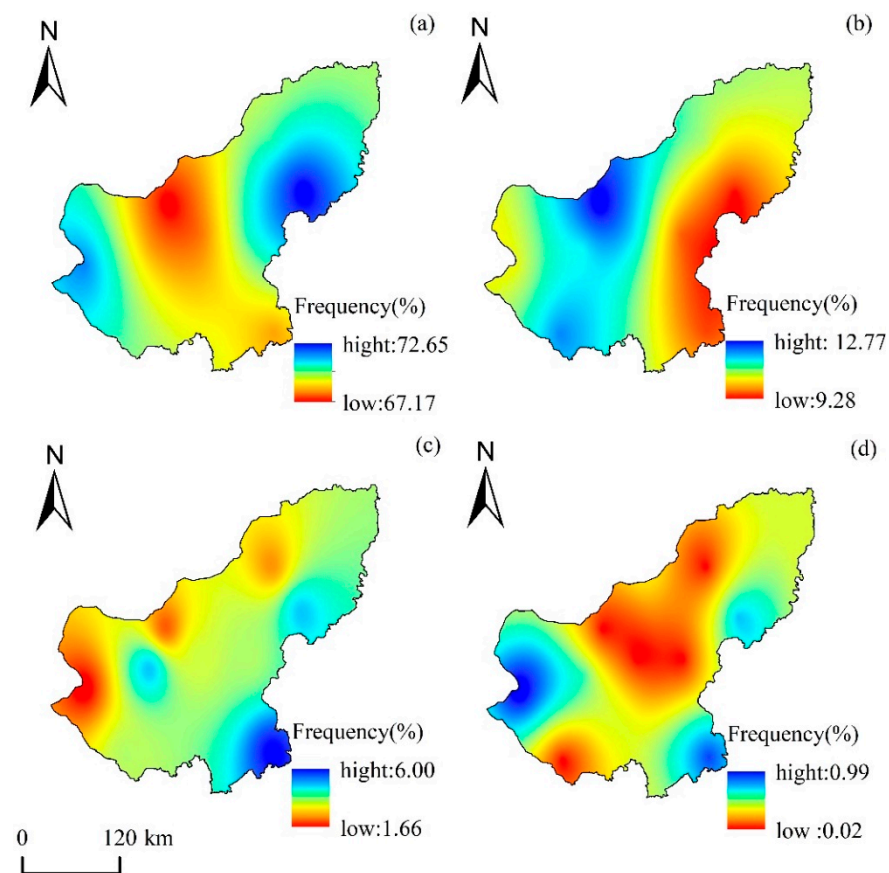


Figure 3. Distribution of the drought frequency in different grades from 1969 to 2018. (a) Normal, (b) mild drought, (c) moderate drought, and (d) severe drought.

It can be seen from Figure 4 that the southwest and middle of Xilin Gol are areas with high drought intensity. It is mainly the high latitude circulation anomaly that leads to the increase in atmospheric pressure, the interdecadal weakening of the East Asian monsoon, and the decrease in northward water vapor, which is represented by the decrease in continuous precipitation days and precipitation intensity [35,36], and finally, the precipitation in Xilin Gol further tends to decline. From March to May, due to scarce rainfall and high soil evaporation, the spatial distribution of drought was large. Among them, the average drought intensity of each meteorological station in April was 8.51, and the number of stations with the drought intensity above the average was five, accounting for about 55.56%, mainly distributed in East Wuzhumuqin Banner in the northeast, Narenbolige in the middle, Erenhot in the southwest, and Zhurihe. The drought intensity of Complerog reached 13.09. There is a large amount of precipitation from June to August, and the nature of precipitation is mainly convective [37], which leads to the drought showing a high distribution in the south and low in the north. From September to December, the spatial distribution of the drought intensity gradually decreased from southwest to northeast, and the high value of the drought intensity appeared in the southwest. In December, the average drought intensity of each meteorological station was 13.65, and the number of stations with drought intensity above the average was four, accounting for about 44.44%. The drought intensity reached 17.24 in Nalemblige, Abaga Banner, and Sunite Left Banner in the central region and Zhurihe in the south.

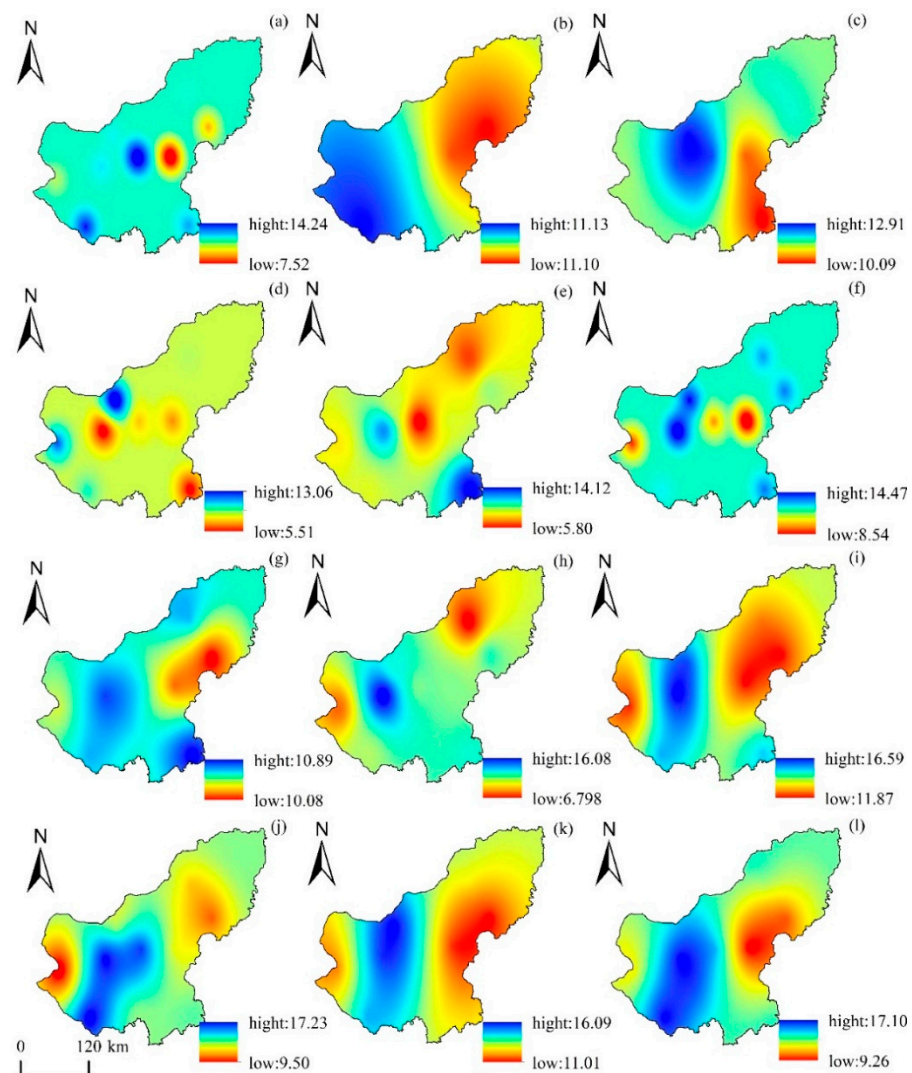


Figure 4. Spatial distribution of scale drought intensity from 1969 to 2018. (a) January, (b) February, (c) March, (d) April, (e) May, (f) June, (g) July, (h) August, (i) September, (j) October, (k) November, and (l) December.

3.1.3. Variation of Drought Trend

Figure 5 shows the spatial distribution of trend change of effective drought index in Xilin Gol from 1969 to 2018, with negative values indicating drought trend and positive values indicating wet trend. The effective drought index has some differences in different months. From January to March, and from September to December, all the nine stations showed a trend of drought. The probability of drought in September–November was higher than that in March–May, showing a very obvious aggravation trend in the whole historical period, and the trend in October was the largest, with a linear rate of $-0.127/10a$. The drought trend was the lowest in February, with a linear rate of $-0.091/10a$. In the 4–9 August precipitation sites, the trend of drought and a moist and humid trend was observed for May and June, respectively, for eight sites, including East Wuzhumuqin, East Wuzhumuqin, Zhurihe, and West Ujimqin, with a maximum linear rate trend of $0.047/10$. Duolun was the wet site in July, and Dongwuzhumuqin Banner and Erenhot were the wet sites in August.

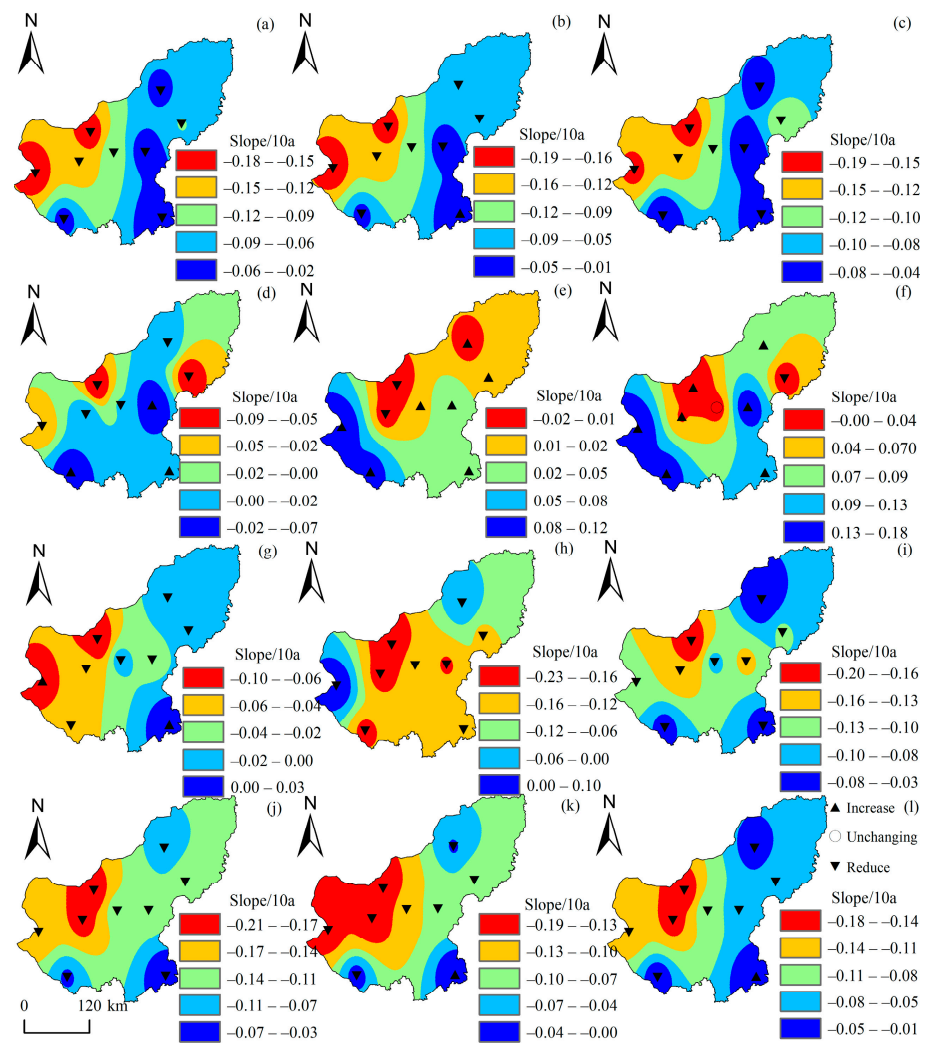


Figure 5. Drought trend variation of stations from 1969 to 2018. (a) January, (b) February, (c) March, (d) April, (e) May, (f) June, (g) July, (h) August, (i) September, (j) October, (k) November, and (l) December.

According to the analysis of the M–K trend test results of an effective drought index, the proportion of stations with increasing drought trend in different months in Xilin Gol was 12.03%. Among them, the proportion of stations with increasing drought trend in different months was 5.55%, and the proportion of stations with increasing drought trend that passed the significance test was 4%. Most of the stations with decreasing trend of drought did not pass the 0.05 significance level test; only Zhurihe and Duolun in June were the exceptions, indicating that most of the stations in Xilin Gol had insignificant changes in the increasing and decreasing trends of drought.

3.1.4. Analysis of Temporal and Spatial Modes of Drought

Table 2 shows the EOF decomposition findings in Xilin Gol. The cumulative variance contribution rate of the first five eigenvalues was 88.81%, but only the first two did not overlap, and the rate was close to 70%. These two eigenvectors can describe the geographical distribution of drought in Xilin Gol from 1969 to 2018.

Table 2. The contribution rate of the first five eigenvectors of EOF decomposition of Xilin Gol annual effective drought index.

Modal	Eigenvalue	Variance Contribution Rate/%	Cumulative Variance Contribution Rate/%	Characteristic Root Error Range	
1	1.76	52.75	52.75	0.93	2.59
2	0.48	14.38	67.13	0.25	0.70
3	0.32	9.60	76.73	0.16	0.47
4	0.22	6.76	83.49	0.11	0.33
5	0.17	5.32	88.81	0.09	0.26

As can be seen from Table 2, the variance contribution rate of the eigenvector in mode 1 is 52.75%, much higher than that of other modes. Therefore, it is considered that the spatial distribution of each component of the eigenvector in Mode 1 is the main spatial distribution type of the meteorological drought field in Xilin Gol. In mode 2, the variance contribution rate of the eigenvector is 14.38%, which is also a typical spatial distribution type of the meteorological drought field in Xilin Gol. According to the above analysis, it is clear that there are two main types of meteorological drought fields in Xilin Gol, namely the uniform type and southeast–northwest inverse-phase type.

Spatial distribution maps of modes 1 and 2 were drawn based on inverse distance weighting (Figure 6). As can be seen from Figure 6a,b, the coefficient of the first eigenvector has a consistent positive distribution with a small difference, indicating that precipitation at each station makes a balanced contribution to drought. The larger values are mainly located in the north of Xilinhot City and Abaga Flag, as well as the south of Zhengxiangbai Flag and Taipishi Flag, with an overall decrease in the east and west directions. The first principal component mainly indicates that the precipitation of Xilinhot City and Abaga Banner in the central part and Zhengxiangbai Banner and Taipu Banner in the south have a greater impact on drought. The spatial variation characteristics represented by the first eigenvector can be regarded as the main form of drought spatial distribution in Xilin Gol League. The spatial distribution of the second eigenvector is generally characterized by the decreasing trend of drought from Sunite Right Banner, Xianghuang Banner, Zhengxiangwhite Banner, Zhenglan Banner, Duolun County, and Taipiliqi in the southwest to the north and northeast counties, and the most arid area is located in Sunite Right Banner. It corresponds to the minimum negative value of -0.44 , and the maximum value is Wulagai area in Eastern Uzhumuqin Banner.

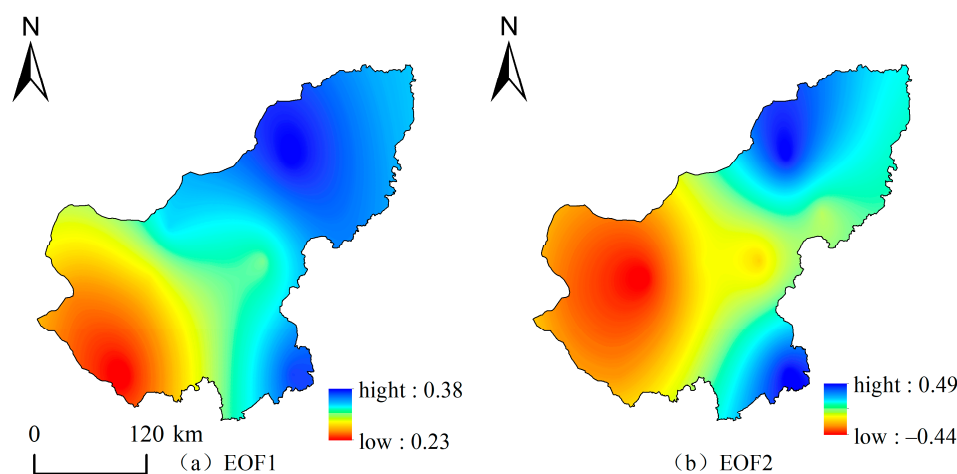


Figure 6. Spatial distribution of the first two eigenvectors of EDI from 1969 to 2018. (a) EOF first mode. (b) EOF second mode.

As can be seen from the time series of the first mode (Figure 7a), the overall trend is decreasing, especially from 2000 to the end of 2010, with a standard deviation of ± 1.34 .

Since this mode has a large weight, it can basically reflect the drought situation of the whole region in each year. From the perspective of individual years, 1970, 1992, and 1998 were much higher than 1.34, indicating that these years were wetter, while the time series of 2001, 2005, 2006, 2007, and 2011 were lower than -1.34 , indicating that the drought was more severe. The time series of the second mode showed an upward trend (Figure 7b), with a standard deviation of ± 0.70 . In terms of individual years, the time series of 1989, 1990, and 2001 were far greater than 0.84 and relatively wet. However, the time series of 1973, 1975, 1976, 1979, 1996, 2009, and 2010 were less than -0.70 and relatively dry. According to the records of Meteorological Disaster Dictionary, 1975, 1976, 1979, 2009, and 2010 were the years of severe drought in Xilin Gol, consistent with the present study and also reflect that the EDI has good adaptability in this region.

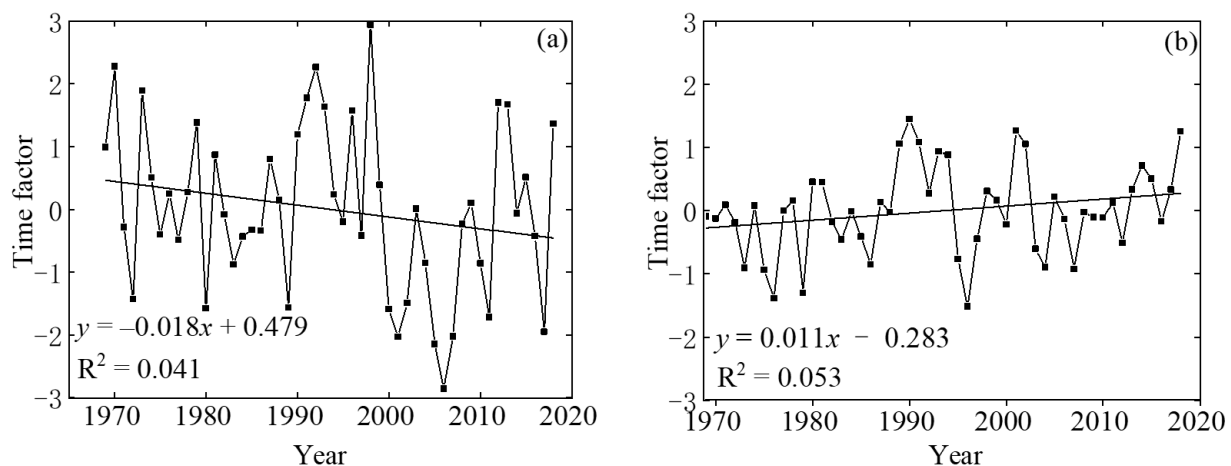


Figure 7. The time coefficients corresponding to the first two feature vectors of the EDI in 1969–2018. (a) Corresponding time coefficients for the first mode of EOF; (b) corresponding time coefficients for the second mode of EOF.

3.2. Characteristics of Vegetation Change in Xilin Gol

Figure 8 shows grassland NDVI fluctuation and distribution in Xilin Gol from 2000 to 2018. Figure 8a shows that the average NDVI of the desert steppe, typical steppe, and meadow steppe has increased over the past 19 years, notably in the typical steppe (0.034/10a). On the whole, the average annual NDVI also fluctuated with a growth rate of 0.021/10a. The minimum (0.358) and maximum (0.508) NDVI values occurred in 2000 and 2018, respectively. Therefore, the vegetation cover of Xilin Gol grassland was improved. As shown in Figure 8b, the mean NDVI of the vegetation in this area ranged from 0 to 1. Affected by grassland types, the NDVI of Xilin Gol showed an increasing spatial distribution pattern from southwest to northeast, with obvious spatial heterogeneity. The low NDVI areas were mainly distributed in desert steppe areas such as Sunite Left Banner, Sunite Right Banner, Erenhot Banner, and Xianghuang Banner. NDVI high values are mainly distributed in meadow steppe and typical steppe areas in East Uzhimuqin Banner and West Ujimqin Banner. It can be seen from Figure 8c that grassland NDVI in Xilin Gol showed an obvious decreasing trend from 2000 to 2018, mainly distributed in typical steppe areas but also in desert areas and meadow steppe areas, with the maximum decreasing rate reaching $-0.042/10a$. The NDVI in the center part of East Uzhumuqin Banner, north of Xilinhote and south of Duolun, increased by 0.031/10a.

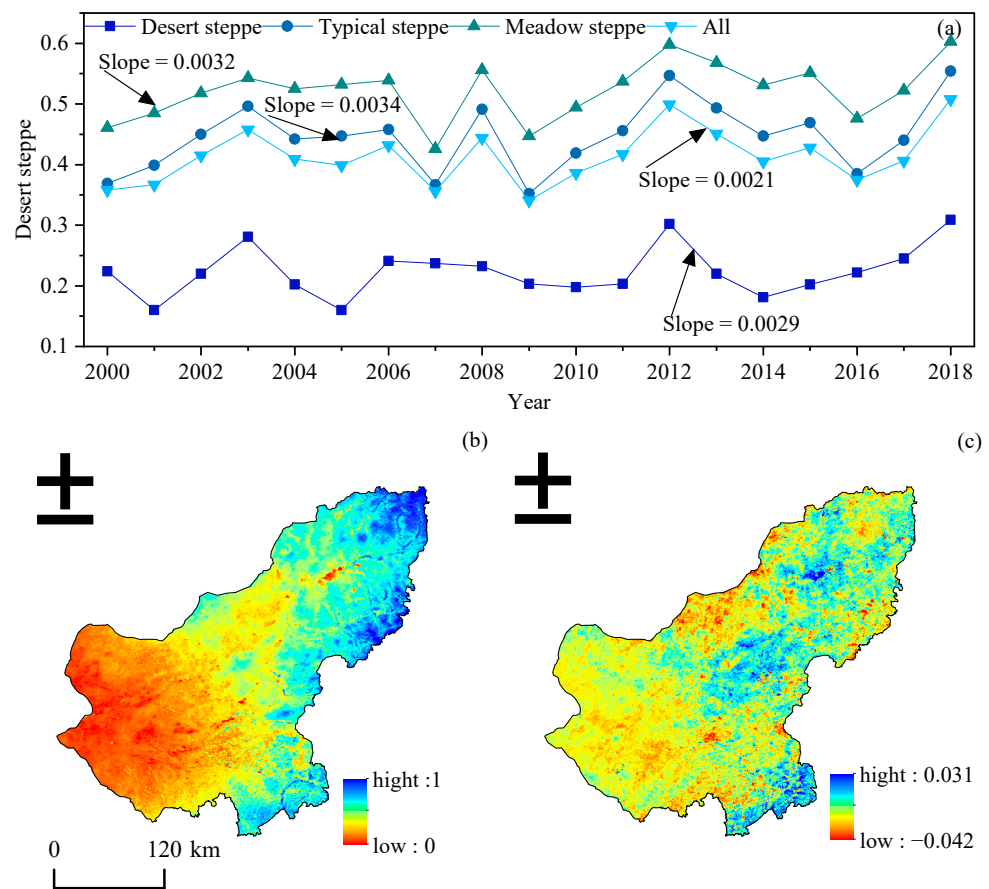


Figure 8. Changes in Xilin Gol's NDVI in space and time from 2000 to 2018: (a) the trend of NDVI change between years in different types of grasslands, (b) the spatial distribution pattern of annual NDVI, and (c) the spatial distribution pattern of the rate of NDVI change.

3.3. Effects of Drought on Vegetation

According to the findings (Figure 9), the geographical distribution of the correlation coefficient between the NDVI and EDI in Xilin Gol varied from -0.642 to 0.888 , and the average correlation coefficient was 0.392 . The correlation coefficient ranged from -0.642 to 0.888 . Only 1.77% of the regions had a negative correlation, while the remaining 98.23% of the regions had a positive correlation. The regions that had a negative connection were primarily dispersed among different kinds, with some typical steppe regions also included. As a whole, the major area included 37.72% of the whole area, while the unimportant area was responsible for 62.28% of the entire area. The correlation coefficient between the NDVI and EDI was 0.386 in the typical steppe, which was the lowest of the three types of steppes studied. The correlation value between the NDVI and EDI was 0.448 in the desert steppe and 0.394 in the meadow steppe. It is clear that the flora that grows in the various types of grasslands has varying degrees of sensitivity to the effects of drought, with the desert steppe being the most vulnerable. The lack of precipitation is the primary reason that inhibits the expansion of vegetation in Xilin Gol, which is located in semi-arid and desert areas. The overall rate of plant development in Xilin Gol was quite sensitive to the level of dryness that was present. The regions of Sunite Left Banner, Sunite Right Banner, and Erenhot were the ones that generally had the highest correlation coefficient between the vegetation index and the EDI. The region known as Duolun has the correlation coefficient with the lowest value.

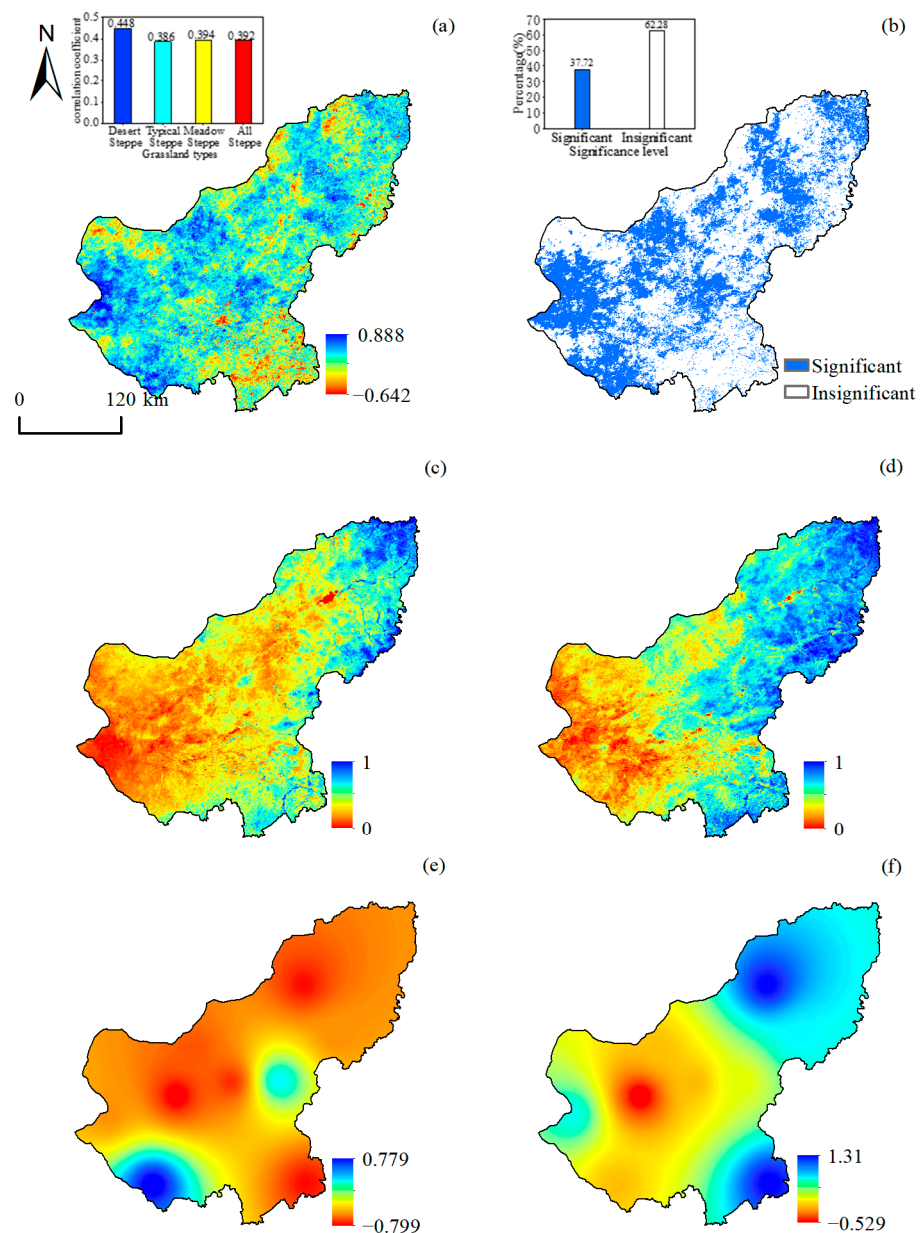


Figure 9. Annual NDVI and EDI correlation coefficient and significance test spatial distribution in Xilin Gol from 2000 to 2018. (a) Spatial distribution of the correlation coefficients, (b) spatial distribution of the significance tests, (c) spatial distribution of the NDVI in 2000, (d) spatial distribution of the NDVI in 2018, (e) spatial distribution of the EDI in 2000, and (f) spatial distribution of the EDI in 2018. (Significant is $p < 0.05$; Insignificant is $p \geq 0.05$).

4. Discussion

The weak decrease in precipitation in Xilin Gol in recent years is believed to be the main cause of the increase in meteorological drought, but the overall trend is similar to the results of [38] in their study on the spatiotemporal distribution characteristics of drought using standardized precipitation evapotranspiration index. Xilin Gol's droughts are regular, long-lasting, and evenly distributed. Severe droughts occur throughout winter, spring, and early summer. Autumn drought has increased in recent years [39]. Due to Westerly circulation and altitude, the dry season after September is characterized by low temperatures, fierce winds, and minimal rain. Through geographical and temporal drought analysis, this research acquired the uniform drought distribution pattern of the whole Xilin Gol and the southeast-northwest antiphase, which was largely compatible with the

constant trend of Xilin Gol League [40]. The number of modes and variance contribution rate function differently due to the drought index and size. The *EDI* can reflect Xilin Gol's spatial and temporal variety, but it has flaws. The temperature, evaporation, sunlight hours, and wind speed also impact drought. The *EDI* is based on monthly precipitation, which cannot represent drought length and alleviation mechanisms. With the spatial variability of climatic factors and the area natural environment, further study is needed to understand the spatial and temporal distribution of drought and its internal mechanism in Xilin Gol.

The NDVI of Xilin Gol was improved overall but deteriorated locally. This is consistent with the research conclusions of [41,42]. Since 2000, Xilin Gol has gradually implemented the policy of returning farmland to forest or grassland. In the past 19 years, have achieved remarkable results, and the vegetation coverage rate has been improved. In the eastern part of Xilin Gol, the vegetation is relatively stable, but there is some attenuation in parts. The overall growth of vegetation in the central region is gentle, and the vegetation in some areas (Duolun County, Taiwusi Banner) is improved. The reason for this is that Taifusi Qi and Duolun County are the key implementation areas of ecological construction projects. The projects are comprehensive, and the implementation effect is good, not only improving the local ecology but also optimizing the industrial structure and promoting economic development [43–46]. The study area is divided into meadow steppe, typical steppe, and desert steppe from east to west. Reference [47] showed that the utilization efficiency of the three types of grassland vegetation to precipitation decreased successively. The authors of [48] believed that different types of grassland resulted in different resilience, stability, and ecological fragility of the ecological environment. the NDVI of meadow steppe, typical steppe, and desert steppe showed an upward trend, especially the improvement trend of typical steppe vegetation. However, the improvement trend of desert steppe vegetation was low, mainly distributed in Sunite Left Banner and Sunite Right Banner. Due to the difference of grassland types, the ecosystem structure was different, so the vegetation coverage was different. Desert steppe is more susceptible to climate change because of its low ability to adapt to climate change.

As a means of coping with the effects of drought, plants are able to slow their rates of photosynthesis, respiration, and overall growth when dry conditions prevail [49]. Since the structure and function of the many forms of vegetation are not identical, these plants have varying degrees of adaptation to the temperature and surroundings [50]. From the point of view of spatial distribution, the correlation between the NDVI and *EDI* was high and significant in the western part of the study area, whereas in the central and southern parts of the study area, the correlation between the NDVI and *EDI* was weak and mostly insignificant. This could be because of the distribution characteristics of precipitation and vegetation types in the study area. Water deficit events were more likely to occur in the western part of the study area than in the eastern part of the study area, and the closer to the western part of the study area, the higher the frequency and intensity of drought. The distribution of precipitation in the study area showed a decreasing trend from east to west, and water deficit events were more likely to occur in the western part of the study area than in the eastern part [51]. Second, when looking at the study area from the perspective of the distribution of the different types of vegetation, the northeastern part of the study area is dominated by typical grassland and meadow grassland, and the growth of vegetation in these areas is more likely to be restricted because of the water conditions [52]. As a result, there is a significant relationship between the NDVI and *EDI* in this region. However, because human activities such as irrigation and fertilization generated favorable circumstances for crop development in the agricultural-dominated regions of Taipusi Qi, Duolun, Zhenglan Qi, and Zhengxiangbai Qi, the association between the NDVI and *EDI* was low in these parts of the region. In general, the NDVI and *EDI* values of the various grassland types in the study area showed a high correlation. This was primarily because the vegetation plants of the various grassland types were small, the roots of herbaceous plants were shallow, and they were sensitive to external environmental disturbance. The accessible water content of the soil decreases during droughts, and the soil normally takes water from

the top and middle layers. Droughts also react very quickly to changes in rainfall. The rapid response of the plant in this area to drought is due to the minimal amount of water that it is able to store; this is the main reason for the rapid response. It is consistent with the conclusion that the vegetation status in the majority of areas in Inner Mongolia is strongly positively connected with drought degree because there is a significant positive correlation between the growth of vegetation and the degree of drought [53]. Due to this, dryness has a dampening impact on the development of plants with shallow root systems.

Despite this, there are still several limitations to the methodology of the research. For instance, after interpolation, the spatial resolution of the *EDI* dataset that was utilized in this work had a lower resolution, and there is a possibility that resampling to the same resolution as the *NDVI* would result in some uncertainties. Additionally, although the distribution of plant types during the time of the research is considered to be constant by default, in reality, the distribution of vegetation shifts as a result of climate change and human activity [54,55]. Previous research demonstrates that the closer the area to the city, the earlier the growing season begins and finishes [56]. Moisture and climate also affect plant development [57,58]. This research solely addresses the *EDI*'s influence on vegetation, and disregarding other factors skews the results. With worsening drought, the lag impact on vegetation lasts longer, whereas the cumulative effect is shorter, and the lag effect intensity on the *NDVI* is significantly smaller than the cumulative effect [59]. Future study must address the aforesaid issues.

5. Conclusions

Using the *EDI*, we looked at how drought changed over time and space in Xilin Gol from 1969 to 2018 and explored the patterns we saw in the drought's temporal and geographical distribution. The following inferences were made:

This study comprehensively describes the severity, frequency, intensity, and geographical extent of drought in Xilin Gol, Inner Mongolia, during the study period (1969–2018). The results showed that the drought degree of the study area increased on the whole, and the *EDI* changed greatly during 1970–1980, indicating that the dry and wet transition occurred in the region. The drought frequency was higher in the west, northwest, and southeast of the study area but lower in the middle and northeast of the study area. The drought frequency in the northwest was higher than that in the west and southeast of the study area. However, the intensity of drought was mainly concentrated in the central, northeastern, and southwestern regions, and the intensity of drought in the southwest and central regions was the highest. In addition, according to the spatial distribution map of the drought index trend variation, the development trend of drought in 12 months of the year was different, showing a trend of aggravating the uneven distribution of the precipitation season, with the largest trend in October at a linear rate of $-0.127/10a$. The trend of drought in February was the smallest at a linear rate of $-0.091/10a$. According to the results of the spatial and temporal mode analysis of drought, there are two main types of meteorological drought fields in Xilin Gol, namely the uniform type and southeast–northwest inverse-phase type. Finally, this study analyzed the spatiotemporal dynamic trend of the *NDVI* of different grassland types and its response to drought from 2000 to 2018 and found that the annual *NDVI* increased by $0.021/10a$. The *NDVI* of the desert steppe, typical steppe, and meadow steppe showed an upward trend, with the most significant increase of $0.034/10a$ in typical steppe. The correlation coefficients between the *NDVI* and *EDI* ranged from -0.642 to 0.888 , with an average of 0.392 . A total of 98.23% of the areas showed positive correlation, and 1.7% showed negative correlation. Most of the negative correlation areas were different species and grasslands. Significant areas accounted for 37.72%, and unrelated areas accounted for 62.28%.

Author Contributions: Methodology, W.L.; software, H.Y.; writing—original draft, Z.C., W.W. and S.Z.; writing—review & editing, Y.W. All authors have read and agreed to the published version of the manuscript.

Funding: This research was funded by the Special Research Project of the China Institute of Water Resources and Hydropower Research (MK2020J11); Inner Mongolia Applied Technology Research and Development fund project (2020GG0020); Inner Mongolia Autonomous Region Key Research and Development and Achievement Transformation plan project (2022YFHH0100); Yinshanbeilu Grassland Eco-Hydrology National Observation and Research Station, and China Institute of Water Resources and Hydropower Research, Beijing 100038, China (grant no YSS202114). The central government guide local funding projects for scientific and technological development (2021ZY0027).

Informed Consent Statement: Not applicable.

Data Availability Statement: Not applicable.

Acknowledgments: The authors are grateful to the editors and the anonymous reviewers for their insightful comments and helpful suggestions.

Conflicts of Interest: The authors declare no conflict of interest.

References

1. Yan, H.; Ran, Q.; Hu, R.; Xue, K.; Zhang, B.; Zhou, S.; Zhang, Z.; Tang, L.; Che, R.; Pang, Z.; et al. Machine learning-based prediction for grassland degradation using geographic, meteorological, plant and microbial data. *Ecol. Indic.* **2022**, *137*, 108738. [[CrossRef](#)]
2. Wu, L.; Liu, H.; Liang, B.; Zhu, X.; Cao, J.; Wang, Q.; Jiang, L.; Cressey, E.L.; Quine, T.A. A process-based model reveals the restoration gap of degraded grasslands in Inner Mongolian steppe. *Sci. Total Environ.* **2022**, *806*, 151324. [[CrossRef](#)] [[PubMed](#)]
3. Wang, X.; Pan, S.; Pan, N.; Pan, P. Grassland productivity response to droughts in northern China monitored by satellite-based solar-induced chlorophyll fluorescence. *Sci. Total Environ.* **2022**, *830*, 154550. [[CrossRef](#)] [[PubMed](#)]
4. Liu, Y.; You, C.; Zhang, Y.; Chen, S.; Zhang, Z.; Li, J.; Wu, Y. Resistance and resilience of grasslands to drought detected by SIF in inner Mongolia, China. *Agric. For. Meteorol.* **2021**, *308–309*, 108567. [[CrossRef](#)]
5. Xu, L.; Chen, N.; Yang, C.; Zhang, C.; Yu, H. A parametric multivariate drought index for drought monitoring and assessment under climate change. *Agric. For. Meteorol.* **2021**, *310*, 108657. [[CrossRef](#)]
6. Li, L.; Qian, R.; Liu, W.; Wang, W.; Biederman, J.A.; Zhang, B.; Kang, X.; Wen, F.; Ran, Q.; Zheng, Z.; et al. Drought timing influences the sensitivity of a semiarid grassland to drought. *Geoderma* **2022**, *412*, 115714. [[CrossRef](#)]
7. Liu, Y.; Dang, C.; Yue, H.; Lyu, C.; Dang, X. Enhanced drought detection and monitoring using sun-induced chlorophyll fluorescence over Hulun Buir Grassland, China. *Sci. Total Environ.* **2021**, *770*, 145271. [[CrossRef](#)]
8. Rascón, J.; Gosgot Angeles, W.; Quiñones Huatangari, L.; Oliva, M.; Barrena Gurbillón, M.Á. Dry and Wet Events in Andean Populations of Northern Peru: A Case Study of Chachapoyas, Peru. *Front. Environ. Sci.* **2021**, *9*, 54. [[CrossRef](#)]
9. Zhang, Y.; Li, Z. Uncertainty Analysis of Standardized Precipitation Index Due to the Effects of Probability Distributions and Parameter Errors. *Front. Earth Sci.* **2020**, *8*, 76. [[CrossRef](#)]
10. Dukat, P.; Bednorz, E.; Ziemblińska, K.; Urbaniak, M. Trends in drought occurrence and severity at mid-latitude European stations (1951–2015) estimated using standardized precipitation (SPI) and precipitation and evapotranspiration (SPEI) indices. *Meteorol. Atmos. Phys.* **2022**, *134*, 20. [[CrossRef](#)]
11. Mallenahalli, N.K. Comparison of parametric and nonparametric standardized precipitation index for detecting meteorological drought over the Indian region. *Theor. Appl. Climatol.* **2020**, *142*, 219–236. [[CrossRef](#)]
12. Choudhury, A.; Dutta, D.; Bera, D.; Kundu, A. Regional variation of drought parameters and long-term trends over India using standardized precipitation evapotranspiration index. *J. Environ. Manag.* **2021**, *296*, 113056. [[CrossRef](#)]
13. Wang, Y.; Liu, G.; Guo, E. Spatial distribution and temporal variation of drought in Inner Mongolia during 1901–2014 using Standardized Precipitation Evapotranspiration Index. *Sci. Total Environ.* **2019**, *654*, 850–862. [[CrossRef](#)] [[PubMed](#)]
14. Zheng, Y.; Zhang, X.; Yu, J.; Xu, Y.; Wang, Q.; Li, C.; Yao, X. Assessing the Joint Impact of Climatic Variables on Meteorological Drought Using Machine Learning. *Front. Earth Sci.* **2022**, *10*, 320. [[CrossRef](#)]
15. Ram, S.; Singh, H.N.; Yadav, R.K.; Varikoden, H.; Nandargi, S.S.; Srivastava, M.K. Variations in vapor pressure and standardized precipitation evapotranspiration index since AD 1861 over the western Himalaya in India: Inference from tree ring-width records. *Theor. Appl. Climatol.* **2020**, *140*, 157–166. [[CrossRef](#)]
16. Asadi Zarch, M.A.; Sivakumar, B.; Sharma, A. Droughts in a warming climate: A global assessment of Standardized precipitation index (SPI) and Reconnaissance drought index (RDI). *J. Hydrol.* **2015**, *526*, 183–195. [[CrossRef](#)]
17. Niu, Q.; Liu, L.; Heng, J.; Li, H.; Xu, Z. A Multi-Index Evaluation of Drought Characteristics in the Yarlung Zangbo River Basin of Tibetan Plateau, Southwest China. *Front. Earth Sci.* **2020**, *8*, 213. [[CrossRef](#)]
18. Hajiabadi, F.; Hassanpour, F.; Yaghoobzadeh, M.; Hammami, H.; Amirabadizadeh, M. Evaluation of drought characterization using SPI and SC-PDSI drought indices in baseline and upcoming periods in Birjand region. *Arab. J. Geosci.* **2021**, *14*, 939. [[CrossRef](#)]
19. Yu, H.; Zhang, Q.; Xu, C.Y.; Du, J.; Sun, P.; Hu, P. Modified Palmer Drought Severity Index: Model improvement and application. *Environ. Int.* **2019**, *130*, 104951. [[CrossRef](#)]

20. Mondol, M.A.H.; Zhu, X.; Dunkerley, D.; Henley, B.J. Observed meteorological drought trends in Bangladesh identified with the Effective Drought Index (EDI). *Agric. Water Manag.* **2021**, *255*, 107001. [[CrossRef](#)]
21. Shaik, R.; N.T., M.; G., S.N. Estimation of annual regional drought index considering the joint effects of climate and water budget for Krishna River basin, India. *Environ. Monit. Assess.* **2020**, *192*, 427. [[CrossRef](#)] [[PubMed](#)]
22. Zhang, Y.; Yu, Z.; Niu, H. Standardized Precipitation Evapotranspiration Index is highly correlated with total water storage over China under future climate scenarios. *Atmos. Environ.* **2018**, *194*, 123–133. [[CrossRef](#)]
23. Byun, H.R.; Kim, D.W. Comparing the Effective Drought Index and the Standardized Precipitation Index. *Options Méditerranéennes Série A Séminaires Méditerranéens* **2010**, *95*, 85–89.
24. Kamruzzaman, M.; Hwang, S.; Cho, J.; Jang, M.W.; Jeong, H. Evaluating the Spatiotemporal Characteristics of Agricultural Drought in Bangladesh Using Effective Drought Index. *Water* **2019**, *11*, 2437. [[CrossRef](#)]
25. Wang, Z.; Huang, Z.; Li, J.; Zhong, R.; Huang, W. Assessing impacts of meteorological drought on vegetation at catchment scale in China based on SPEI and NDVI. *Trans. Chin. Soc. Agric. Eng.* **2016**, *32*, 177–186.
26. Hossain, M.L.; Li, J. NDVI-based vegetation dynamics and its resistance and resilience to different intensities of climatic events. *Glob. Ecol. Conserv.* **2021**, *30*, e01768. [[CrossRef](#)]
27. Wang, S.; Li, R.; Wu, Y.; Zhao, S. Effects of multi-temporal scale drought on vegetation dynamics in Inner Mongolia from 1982 to 2015, China. *Ecol. Indic.* **2022**, *136*, 108666. [[CrossRef](#)]
28. Li, J.; Wang, Y.; Liu, L. Responses of the Terrestrial Ecosystem Productivity to Droughts in China. *Front. Earth Sci.* **2020**, *8*, 59. [[CrossRef](#)]
29. Li, C.; Wang, J.; Yin, S.; Bao, Y.; Li, Y.; Yu, S. Drought hazard assessment and possible adaptation options for typical steppe grassland in Xilingol League, Inner Mongolia, China. *Theor. Appl. Climatol.* **2019**, *136*, 1339–1346. [[CrossRef](#)]
30. Tong, S.; Bao, Y.; Te, R.; Ma, Q.; Ha, S.; Lusi, A. Analysis of Drought Characteristics in Xilingol Grassland of Northern China Based on SPEI and Its Impact on Vegetation. *Math. Probl. Eng.* **2017**, *2017*, 5209173. [[CrossRef](#)]
31. Deo, R.C.; Byun, H.-R.; Adamowski, J.F.; Begum, K. Application of effective drought index for quantification of meteorological drought events: A case study in Australia. *Theor. Appl. Climatol.* **2016**, *128*, 359–379. [[CrossRef](#)]
32. Gocic, M.; Trajkovic, S. Analysis of changes in meteorological variables using Mann-Kendall and Sen's slope estimator statistical tests in Serbia. *Glob. Planet. Chang.* **2013**, *100*, 172–182. [[CrossRef](#)]
33. Ionita, M.; Caldarescu, D.E.; Nagavciuc, V. Compound Hot and Dry Events in Europe: Variability and Large-Scale Drivers. *Front. Clim.* **2021**, *3*, 688991. [[CrossRef](#)]
34. Özger, M.; Başakin, E.E.; Ekmekcioğlu, Ö.; Hacısüleyman, V. Comparison of wavelet and empirical mode decomposition hybrid models in drought prediction. *Comput. Electron. Agric.* **2020**, *179*, 105851. [[CrossRef](#)]
35. Yong, M.; Shinoda, M.; Nandintsetseg, B.; Bi, L.; Gao, H.; Wang, Y. Impacts of Land Surface Conditions and Land Use on Dust Events in the Inner Mongolian Grasslands, China. *Front. Ecol. Evol.* **2021**, *9*, 664900. [[CrossRef](#)]
36. Wang, S.; Li, R.; Wu, Y.; Zhao, S. Vegetation dynamics and their response to hydrothermal conditions in Inner Mongolia, China. *Glob. Ecol. Conserv.* **2022**, *34*, e02034. [[CrossRef](#)]
37. Tong, S.; Li, X.; Zhang, J.; Bao, Y.; Bao, Y.; Na, L.; Si, A. Spatial and temporal variability in extreme temperature and precipitation events in Inner Mongolia (China) during 1960–2017. *Sci. Total Environ.* **2019**, *649*, 75–89. [[CrossRef](#)]
38. Zhang, X.; Pan, X.; Xu, L.; Wei, P.; Yin, Z.; Shao, C. Analysis of spatio-temporal distribution of drought characteristics based on SPEI in Inner Mongolia during 1960–2015. *Trans. Chin. Soc. Agric. Eng.* **2017**, *33*, 190–199.
39. Li, W.; Duan, L.; Wang, W.; Wu, Y.; Liu, T.; Quan, Q.; Chen, X.; Yin, H.; Zhou, Q. Spatiotemporal characteristics of drought in a semi-arid grassland over the past 56 years based on the Standardized Precipitation Index. *Meteorol. Atmos. Phys.* **2020**, *133*, 41–54. [[CrossRef](#)]
40. Qiaofeng, Z.; Guixiang, L.; Hongbo, Y.U.; Yuhai, B. Analysis of drought characteristics in Xilingol League based on standardized precipitation index. *J. Nat. Disasters* **2015**, *24*, 119–128.
41. Hang, Y.L.; Bao, G.; Bao, Y.H.; Burenjirigala; Dorjsuren, A. Spatiotemporal Changes of Vegetation Coverage in Xilin Gol Grassland and Its Responses to Climate Change during 2000–2010. *Acta Agrestia Sin.* **2014**, *22*, 1194–1204.
42. Shi, N.N.; Xiao, N.W.; Wang, Q.; Han, Y.; Gao, X.Q.; Feng, J.; Quan, Z.J. Spatio-temporal dynamics of normalized differential vegetation index and its driving factors in Xilin Gol, China. *Chin. J. Plant Ecol.* **2019**, *43*, 331–341. [[CrossRef](#)]
43. Dong, Z.; Rong, A.; Zhang, J.; Tong, Z.; Han, A.; Zhi, F. Study on the Evolutionary Features and Driving Factors of Land-Use System in Xilingol, China. *Land* **2022**, *11*, 526. [[CrossRef](#)]
44. Li, Q.; Wang, J.; Xie, H.; Ochir, A.; Davaasuren, D.; Chen, M.H. Applicability of Grassland Production Estimation Using Remote Sensing for the Mongolian Plateau by Comparing Typical Regions in China and Mongolia. *Sustainability* **2022**, *14*, 3122. [[CrossRef](#)]
45. Dou, H.; Li, X.; Gong, J.; Wang, H.; Tian, Y.; Xuan, X.; Wang, K. Enhanced Ecosystem Services in China's Xilingol Steppe during 2000–2015: Towards Sustainable Agropastoralism Management. *Remote Sens.* **2022**, *14*, 738. [[CrossRef](#)]
46. Fang, A.; Dong, J.; Cao, Z.; Zhang, F.; Li, Y. Tempo-Spatial Variation of Vegetation Coverage and Influencing Factors of Large-Scale Mining Areas in Eastern Inner Mongolia, China. *Multidiscip. Digit. Publ. Inst.* **2019**, *17*, 47. [[CrossRef](#)]
47. Zhang, Y.; Zhang, J.; Xia, J.; Guo, Y.; Fu, Y.H. Effects of Vegetation Phenology on Ecosystem Water Use Efficiency in a Semiarid Region of Northern China. *Front. Plant Sci.* **2022**, *13*, 945582. [[CrossRef](#)]
48. Li, M.; Wang, X.; Chen, J. Assessment of Grassland Ecosystem Services and Analysis on Its Driving Factors: A Case Study in Hulunbuir Grassland. *Front. Ecol. Evol.* **2022**, *10*, 25. [[CrossRef](#)]

49. Gutierrez-Cori, O.; Espinoza, J.C.; Li, L.Z.X.; Wongchuig, S.; Arias, P.A.; Ronchail, J.; Segura, H. On the Hydroclimate-Vegetation Relationship in the Southwestern Amazon During the 2000–2019 Period. *Front. Water* **2021**, *3*, 648499. [[CrossRef](#)]
50. Lv, Y.; Zhao, X.Q.; Zhang, S.R.; Zhang, J.G.; Yue, K.T.; Meng, B.P.; Li, M.; Cui, W.X.; Sun, Y.; Zhang, J.G.; et al. Herbaceous Dominant the Changes of Normalized Difference Vegetation Index in the Transition Zone Between Desert and Typical Steppe in Inner Mongolia, China. *Front. Plant Sci.* **2022**, *12*, 832044. [[CrossRef](#)]
51. Yang, S.; Quan, Q.; Liang, W.; Liu, T. Characteristics of Agricultural Droughts and Spatial Stratified Heterogeneity and Dependence of Dominant Factors in Inner Mongolia Autonomous Region, China. *Atmosphere* **2021**, *12*, 1249. [[CrossRef](#)]
52. Liu, X.; Tian, Y.; Liu, S.; Jiang, L.; Mao, J.; Jia, X.; Zha, T.; Zhang, K.; Wu, Y.; Zhou, J. Time-Lag Effect of Climate Conditions on Vegetation Productivity in a Temperate Forest–Grassland Ecotone. *Forests* **2022**, *13*, 1024. [[CrossRef](#)]
53. Wei, Y.; Zhu, L.; Chen, Y.; Cao, X.; Yu, H. Spatiotemporal Variations in Drought and Vegetation Response in Inner Mongolia from 1982 to 2019. *Remote Sens.* **2022**, *14*, 3803. [[CrossRef](#)]
54. Zhang, H.; Zhang, X.; Shang, Y.; Kattel, G.; Miao, L. Continuously Vegetation Greening over Inner Mongolia for the Past Three Decades. *Remote Sens.* **2021**, *13*, 2446. [[CrossRef](#)]
55. Guo, E.; Wang, Y.; Wang, C.; Sun, Z.; Bao, Y.; Mandula, N.; Jirigala, B.; Bao, Y.; Li, H. NDVI Indicates Long-Term Dynamics of Vegetation and Its Driving Forces from Climatic and Anthropogenic Factors in Mongolian Plateau. *Remote Sens.* **2021**, *13*, 688. [[CrossRef](#)]
56. Kang, W.; Wang, T.; Liu, S. The Response of Vegetation Phenology and Productivity to Drought in Semi-Arid Regions of Northern China. *Remote Sens.* **2018**, *10*, 727. [[CrossRef](#)]
57. Zhu, W.; Wang, S.; Luo, P.; Zha, X.; Cao, Z.; Lyu, J.; Zhou, M.; He, B.; Nover, D. A Quantitative Analysis of the Influence of Temperature Change on the Extreme Precipitation. *Atmosphere* **2022**, *13*, 612. [[CrossRef](#)]
58. Meng, F.; Luo, M.; Sa, C.; Wang, M.; Bao, Y. Quantitative assessment of the effects of climate, vegetation, soil and groundwater on soil moisture spatiotemporal variability in the Mongolian Plateau. *Sci. Total Environ.* **2022**, *809*, 152198. [[CrossRef](#)]
59. Ma, X.-Q.; Leng, P.; Liao, Q.-Y.; Geng, Y.-J.; Zhang, X.; Shang, G.-F.; Song, X.; Song, Q.; Li, Z.-L. Prediction of vegetation phenology with atmospheric reanalysis over semiarid grasslands in Inner Mongolia. *Sci. Total Environ.* **2022**, *812*, 152462. [[CrossRef](#)]